
A fault slip model to study earthquakes due to pore pressure perturbations

Saumik Dana
University of Southern California
Los Angeles, CA 90007
sdana@usc.edu

Birendra Jha
University of Southern California
Los Angeles, CA 90007
bjha@usc.edu

ABSTRACT

The burgeoning need to sequester anthropogenic CO₂ for climate mitigation and the need for energy sustenance leading upto enhanced geothermal energy production has made it incredibly critical to study potential earthquakes due to fluid activity in the subsurface. These earthquakes result from reactivation of faults in the subsurface due to pore pressure perturbations. In this work, we provide a framework to model fault slip due to pore pressure change leading upto quantifying the earthquake magnitude.

1 Introduction

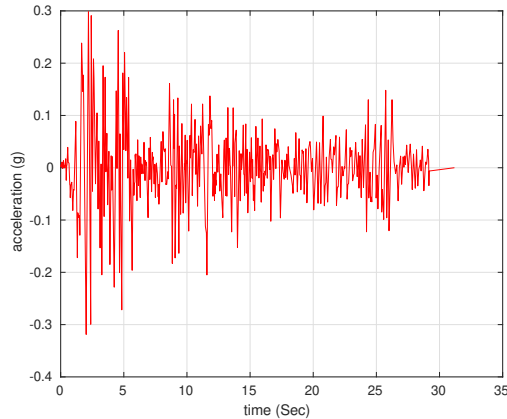


Figure 1: 1940 El Centro earthquake. Accelerogram (measured as normalized to acceleration due to gravity $g = 9.8 \text{ m/s}^2$)

Earthquakes occur as a result of global plate motion. Some plate boundaries glide past each other smoothly, while others are punctuated by catastrophic failures. Some earthquakes stop after only a few hundred metres while others continue rupturing for a thousand kilometres. The simplest model for earthquake initiation is to assume that when the stress accumulated in the plates exceeds some failure criterion on a fault plane, an earthquake happens [1]. Evaluating this criterion requires both a measure of the resolved stress on the fault plane and a quantifiable model for the failure threshold. The groundbreaking work of [2] started with the fact that any stress field can be completely described by its principal stresses, which are given by the eigenvectors of the stress tensor and are interpretable as the normal stresses in three orthogonal directions.

He then proposed that: (1) the stress state could be resolved by assuming that one principal stress is vertical since the Earth's surface is a free surface and (2) faulting occurs when the resolved shear stress exceeds the internal friction on some plane in the medium. Internal friction is defined analogously with conventional sliding friction as a shear stress proportional to the normal stress on a plane. One complication to this simple picture was recognized early on. High fluid pressures can support part of the load across a fault and reduce the friction. The importance of the fluid effect on fault friction was first recognized by [3]. In the course of their work on oil exploration, they observed that pressures in pockets of fluids in the crust commonly exceeded hydrostatic pressure. They connected this observation with studies of faulting and proposed that the pore pressure at a depth can approach the normal stress on faults, resulting in low friction. Fig. 1 shows the seismograph recorded acceleration of the 1940 EL Centro earthquake that occurred in the Imperial Valley in southeastern Southern California near the USA-Mexico border. It was the first major earthquake to be recorded by a strong-motion seismograph located next to a fault rupture, and led to a total damage of \$6 million [4].

1.1 Enhanced geothermal systems (EGS)

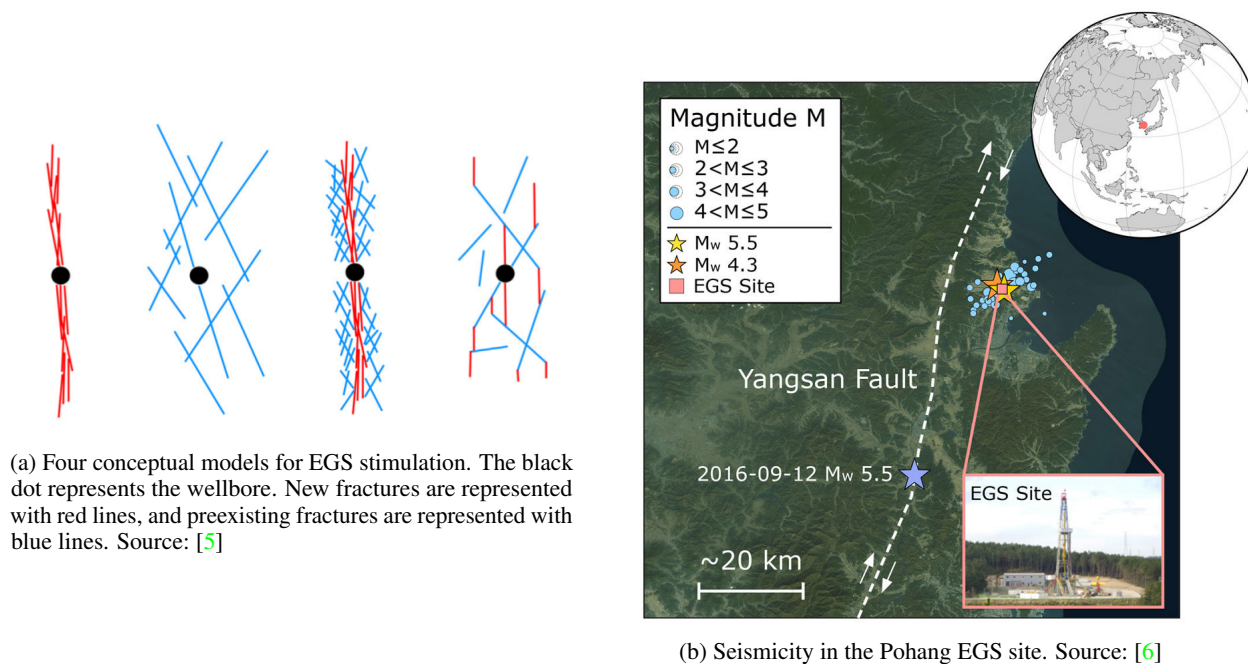


Figure 2: EGS

Pulse fracturing in hot dry rock is a complex multi-physics problem which involves nucleation and propagation of cracks by injecting a combination of padding fluid/proppant/propellant at high pressure down a wellbore [7–16], and has documented long lasting implications for EGS [5, 9, 17–19]. As shown in Fig. 2a, the conceptual models that have been proposed in literature as stimulation mechanisms in EGS [5] include (1) Only new, propagating fractures contribute to permeability enhancement, (2) Stimulation occurs only through induced slip on preexisting fractures, (3) Continuous new fractures propagate away from the wellbore, but fluid leaks off into natural fractures, which slip and experience enhanced transmissivity, and (4) Continuous pathways for flow involve both new and preexisting fractures. The fourth mechanism has been widely accepted to model hydraulic stimulation of EGS [20–23]. The fracture initiated from a sheared preexisting natural fracture is called a wing crack or a splay fracture. Wing cracks found in rock are tensile fractures but they are different from hydraulic fractures because (1) wing cracks are initiated from the tension field induced by shear slip of a preexisting natural fracture while hydraulic fractures are initiated from an injection well by fluid pressure; (2) wing cracks are curved cracks while hydraulic fractures propagate straight and perpendicularly to the least principal stress; and (3) tension forces to open wing cracks are supported both by fluid pressure and shear slip of a preexisting natural fracture while tension forces to open hydraulic fractures are supported only by fluid pressure [23]. Hitherto, HF has been associated with microseismic events due to their small magnitudes.

However, there is now growing evidence to suggest that HF induced fault activity in EGS projects across the world has caused larger earthquakes [6, 20, 22]. Fig. 2b shows the distribution of seismicity in the Pohang, South Korea EGS site. Postulates suggest the actual amount of injected fluid was only 0.2% of what is theoretically expected for the largest recorded earthquake at the site [6, 24]. The causation is established via spatio-temporal correlation; the events occur close (< 10 km) to the injection well and shortly (minutes to hours) after injection. Most of the sites are in geographical regions with little to no history of prior natural seismicity, which further supports the causative link between fracturing and the observed seismic events.

1.2 Earthquake triggering mechanisms

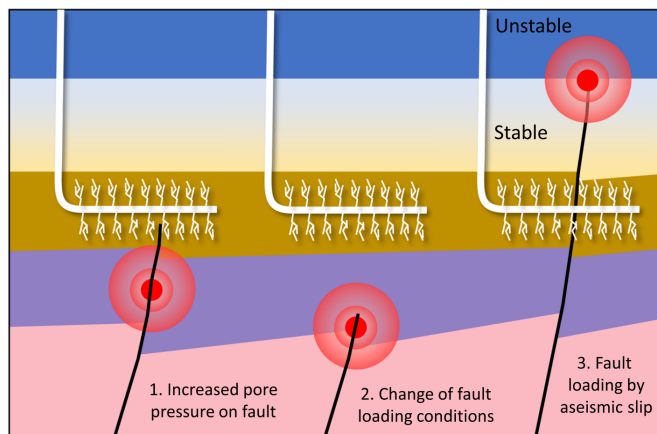


Figure 3: Three proposed earthquake triggering mechanisms in literature. Source: [24]

The earthquake triggering mechanisms (see Fig. 3) that have been proposed are: (1) propagation of the fluid pressure diffusion front through the newly created fracture network, followed by pressurization/lubrication of a basement fault that slips seismically [25], (2) poroelastic stress transfer from slipped fractures on to the fault causing an increase in shear and/or tension on the fault followed by seismic slip, and (3) fluid injection-induced aseismic rupture front which propagates faster and to larger distances than the fluid pressure diffusion front, thereby transmitting stresses to unstable portions of the fault beyond the fluid-pressurized region [26]. All three mechanisms can activate a critically stressed fault (initial stress state close to frictional failure), which can culminate into an induced seismic event [24, 27–34]. In quasi-static simulations, which neglect elastodynamics and wave propagation effects, the induced seismicity mechanisms are often quantified using Coulomb Failure Function (CFF) [35–37], which includes contributions from the effective stress and fault’s friction coefficient. The effective stress is defined as the difference between the total stress (from tectonics and expansion/contraction of surrounding rock) and the pore pressure (from injection) scaled by the Biot coefficient. The friction coefficient evolution often requires a fault rheological model e.g., the Slip Weakening or the Rate- and State-dependent Friction (RSF) model. RSF is the gold standard for modeling earthquake cycles (inter-seismic loading followed by co-seismic relaxation) on faults [38–40], whereas slip weakening provides a reasonable approximation for modeling the drop in friction during a single seismic/aseismic event. CFF is computed using the fault traction vector which is given by the product of the effective stress tensor and the fault normal vector. Initially, when the fault is locked and under equilibrium with the tectonic and hydrostatic stresses, $CFF < 0$. As injection proceeds, the pore pressure increases and the near-wellbore region expands volumetrically, which applies compression on the region farther from the wellbore. The spatial distribution of the total stress tensor and pressure around the fault change. An increase in CFF, i.e. $\Delta CFF > 0$, indicates fluid-induced destabilization of the fault. When CFF exceeds fault’s intrinsic cohesion, the fault may slip. The slip releases the host rock strain energy, accumulated from natural and/or anthropogenic loading, over multiple years. The slip can be seismic or aseismic depending on fault’s frictional properties (e.g., velocity-weakening vs. velocity-strengthening) and the fault loading rate. Similarly, a decrease in fault’s CFF, e.g., due to stresses transferred from a newly created HF, can induce mechanical stabilization of the fault.

2 Fault slip model

Elastodynamics [41, 42] and quasi-dynamic [43, 44] approaches allow calculation of the seismic magnitude from dynamic fault rupture simulations [45–50]. Elastodynamics includes the inertia term in the equilibrium equation, whereas quasi-dynamic approximates inertial effects via a radiation damping term [51].

2.1 Displacement discontinuity

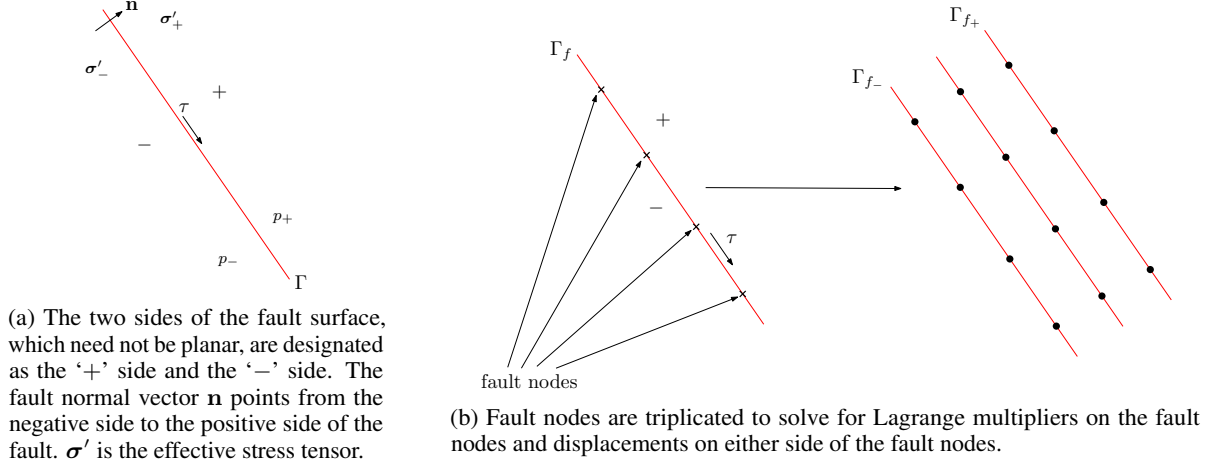


Figure 4: Fault mechanics

As shown in Figs. 4a and 4b, we treat faults as surfaces of discontinuity embedded in the continuum across which displacement is allowed to be discontinuous to recognize the possibility of fault slip [36, 52]. Slip on the fault is the displacement of the positive side relative to the negative side,

$$(\mathbf{u}_+ - \mathbf{u}_-) - \mathbf{d} = \mathbf{0} \text{ on } \Gamma_f, \quad (1)$$

where \mathbf{d} is the fault slip vector. We impose the effective traction on the fault by introducing a Lagrange multiplier, \mathbf{l} , which is a force per unit area required to satisfy Eq. (1). A positive value of $\mathbf{l} \cdot \mathbf{n}$ indicates that a tensile effective stress is transmitted across the fault surface. The Kuhn-Tucker conditions of contact mechanics are obeyed such that no penetration occurs and the effective normal traction stays compressive at the contact surface.

2.2 Fault traction

The shear traction on the fault is computed as

$$\tau = |\mathbf{l} - (\mathbf{l} \cdot \mathbf{n})\mathbf{n}| \quad (2)$$

We use the Mohr-Coulomb theory to define the stability criterion for the fault [53]. When the shear traction on the fault is below the friction stress, $\tau \leq \tau_f$, the fault does not slip. When the shear traction is larger than the friction stress, $\tau > \tau_f$, the contact problem is solved to determine the Lagrange multipliers and slip on the fault, such that the Lagrange multipliers are compatible with the frictional stress [36].

2.3 Fault friction

The frictional stress τ_f on the fault as

$$\tau_f = \begin{cases} \tau_c - \mu \mathbf{l} \cdot \mathbf{n}, & \mathbf{l} \cdot \mathbf{n} < 0, \\ \tau_c, & \mathbf{l} \cdot \mathbf{n} \geq 0, \end{cases} \quad (3)$$

where τ_c is the cohesive strength of the fault and μ is the coefficient of friction. The rate- and state-dependent friction model [38, 39, 54–56] is

$$\begin{aligned}\mu &= \mu_0 + A \ln \left(\frac{V}{V_0} \right) + B \ln \left(\frac{V_0 \theta}{d_c} \right), \\ \frac{d\theta}{dt} &= 1 - \frac{\theta V}{d_c},\end{aligned}\tag{4}$$

where $V = |d\mathbf{d}/dt|$ is the slip rate magnitude, μ_0 is the steady-state friction coefficient at the reference slip rate V_0 , A and B are empirical dimensionless constants, θ is the macroscopic variable characterizing state of the surface and d_c is a critical slip distance. Here, θ may be understood as the frictional contact time [38], or the average maturity of contact asperities between the sliding surfaces [51]. The evolution of θ is assumed to be independent of changes in the normal traction that can accompany the fault slip due to changes in fluid pressure. The model accounts for the decrease in friction (slip-weakening) as the slip increases, and the increase in friction (healing) as the time of contact or slip velocity increase. The two effects act together such that $A > B$ leads to strengthening of the fault, stable sliding and creeping motion, and $A < B$ leads to weakening of the fault, frictional instability, and accelerating slip. In this way, the model is capable of capturing repetitive stick-slip behavior of faults and the resulting seismic cycle [39, 55].

2.4 Fault pressure

A difference in fluid pressure across the fault leads to a pressure jump $[[p]]_\Gamma = p_+ - p_-$, where p_+ and p_- are the equivalent multiphase pressures on the ‘positive’ and the ‘negative’ side of the fault. This pressure jump leads to a discontinuity in the effective stress across the fault, such that the total stress is continuous,

$$\boldsymbol{\sigma}'_- \cdot \mathbf{n} - b p_- \mathbf{n} = \boldsymbol{\sigma}'_+ \cdot \mathbf{n} - b p_+ \mathbf{n},\tag{5}$$

where b is the Biot coefficient. Fault stability can be assessed by evaluating the stability criterion on both sides of the fault separately. The side of the fault where the criterion is met first determines the fault stability. Equivalently, this can be achieved by defining a *fault pressure* that is a function of the pressures on the two sides, p_+ and p_- . Introducing the fault pressure allows us to uniquely define the *effective* normal traction on the fault, σ'_n , and determine the fault friction τ_f (Eq. (3)). Since the stability criterion $\tau > \tau_f$ is first violated with the larger pressure, we define the fault pressure p as

$$p = \max(p_-, p_+).\tag{6}$$

2.5 Earthquake magnitude

In case of the elastodynamics framework with the RSF fault model, once the slip is nucleated at the hypocenter, wave propagation is simulated during seismic slip. Depending on the hypocenter location, the natural fractures, HF, distant portions of the fault, and reservoir boundaries can act as barriers to the seismic wave fronts. Such barriers can be treated as inclusions using absorbing boundary layers (ABLs) [57] or perfectly matched layers (PMLs) [58, 59]. The moment-based seismic magnitude [60] is computed as $M_w = \frac{2}{3} \log_{10} M_0 - 6.0$, where the seismic moment is $M_0 = \int_{\Gamma_f} G |\mathbf{d}| d\Gamma$, $|\mathbf{d}|$ is the magnitude of the slip vector (accumulated over the event duration).

3 Numerical challenges

As shown in Fig. 5, we deploy the fixed stress split algorithm [61–70] in the open source geodynamics framework [52, 71] coupled with a multiphase flow code [36] to solve the coupled problem. While it is well-known that the multiphase flow problem brings in a host of numerical issues associated with the simultaneous resolution of pressure-saturation primary variables [72–75], the presence of faults renders the geomechanics as a saddle point problem. Although the geodynamics framework handles the saddle point problem efficiently, the coupling with the multiphase flow code brings in a set of challenges that require careful consideration of the solvers deployed for both flow and geomechanics. In addition to that, the elastodynamics brings in time stepping issues associated with the explicit update of the displacement primary variable. We shall tackle all these challenges in future work.

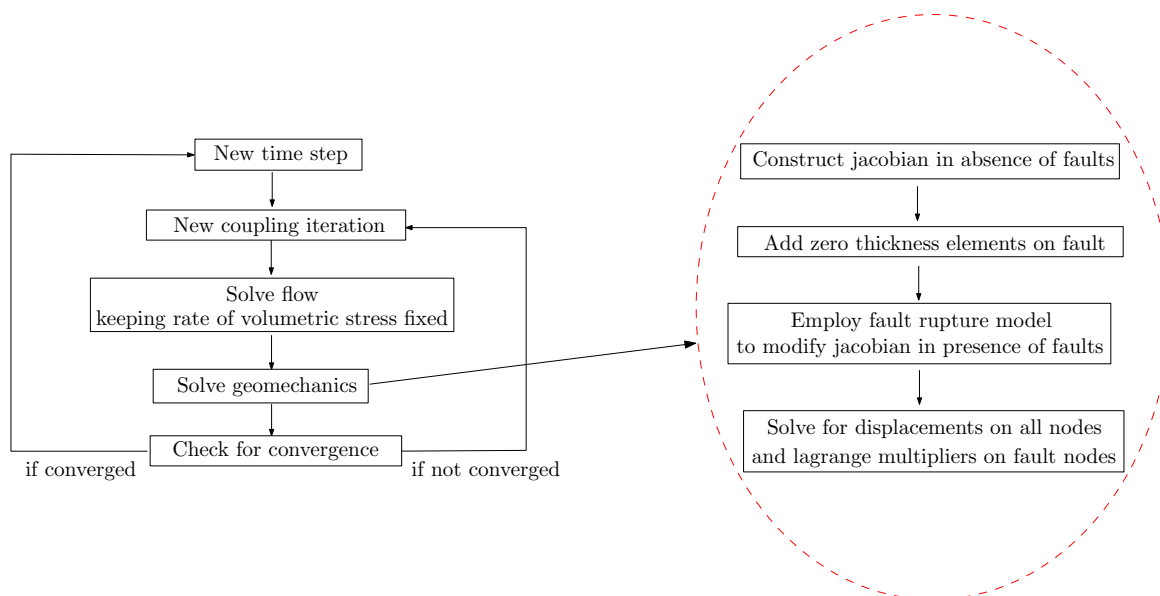


Figure 5: Algorithmic flowchart

References

- [1] Hiroo Kanamori and Emily E Brodsky. The physics of earthquakes. *Reports on Progress in Physics*, 67(8):1429, 2004.
- [2] Ernest Masson Anderson. The dynamics of faulting. *Transactions of the Edinburgh Geological Society*, 8(3):387–402, 1905.
- [3] M King Hubbert and William W Rubey. Role of fluid pressure in mechanics of overthrust faulting: I. mechanics of fluid-filled porous solids and its application to overthrust faulting. *Geological Society of America Bulletin*, 70(2):115–166, 1959.
- [4] Carl W Stover and Jerry L Coffman. *Seismicity of the United States, 1568-1989 (revised)*. US Government Printing Office, 1993.
- [5] Mark W McClure and Roland N Horne. An investigation of stimulation mechanisms in enhanced geothermal systems. *International Journal of Rock Mechanics and Mining Sciences*, 72:242–260, 2014.
- [6] Francesco Grigoli, Simone Cesca, Antonio Pio Rinaldi, A Manconi, Jose Angel Lopez-Comino, JF Clinton, R Westaway, C Cauzzi, Torsten Dahm, and Stefan Wiemer. The november 2017 mw 5.5 pohang earthquake: A possible case of induced seismicity in south korea. *Science*, 360(6392):1003–1006, 2018.
- [7] M King Hubbert and David G Willis. Mechanics of hydraulic fracturing. *Transactions of the AIME*, 210(01):153–168, 1957.
- [8] Carl T Montgomery, Michael B Smith, et al. Hydraulic fracturing: history of an enduring technology. *Journal of Petroleum Technology*, 62(12):26–40, 2010.
- [9] George Everette King et al. Thirty years of gas shale fracturing: What have we learned? In *SPE annual technical conference and exhibition*. Society of Petroleum Engineers, 2010.
- [10] Joel Adams, Clem Rowe, et al. Differentiating applications of hydraulic fracturing. In *ISRM International Conference for Effective and Sustainable Hydraulic Fracturing*. International Society for Rock Mechanics and Rock Engineering, 2013.
- [11] Andrei A Osipov. Fluid mechanics of hydraulic fracturing: a review. *Journal of petroleum science and engineering*, 156:513–535, 2017.
- [12] Zeeshan Tariq, Mohamed Mahmoud, Abdulazeez Abdurraheem, Ayman Al-Nakhli, Mohammed Bataweel, et al. A review of pulse fracturing treatment: an emerging stimulation technique for

- unconventional reservoirs. In *SPE Middle East Oil and Gas Show and Conference*. Society of Petroleum Engineers, 2019.
- [13] BW White, OY Vorobiev, SDC Walsh, et al. Modeling dynamic stimulation of geological resources. In *48th US Rock Mechanics/Geomechanics Symposium*. American Rock Mechanics Association, 2014.
- [14] Matin Parchei-Esfahani, Bruce Gee, and Robert Gracie. Dynamic hydraulic stimulation and fracturing from a wellbore using pressure pulsing. *Engineering Fracture Mechanics*, 235:107152, 2020.
- [15] Arno Zang, Ove Stephansson, and Günter Zimmermann. Keynote: fatigue hydraulic fracturing. *Procedia engineering*, 191:1126–1134, 2017.
- [16] Di Wang, Haibo Wang, Fengxia Li, Mian Chen, and Andrew P Bunger. Parameters affecting the distribution of pulsed proppant in hydraulic fractures. *Journal of Petroleum Science and Engineering*, 191:107125, 2020.
- [17] Mengying Li and Noam Lior. Analysis of hydraulic fracturing and reservoir performance in enhanced geothermal systems. *Journal of Energy Resources Technology*, 137(4), 2015.
- [18] Kagan Kutun. *Hydraulic fracture modeling of an enhanced geothermal system (EGS) experiment*. PhD thesis, Colorado School of Mines, 2018.
- [19] Arno Zang, Günter Zimmermann, Hannes Hofmann, Ove Stephansson, Ki-Bok Min, and Kwang Yeom Kim. How to reduce fluid-injection-induced seismicity. *Rock Mechanics and Rock Engineering*, 52(2):475–493, 2019.
- [20] Amirhossein Kamali and Ahmad Ghassemi. Analysis of injection-induced shear slip and fracture propagation in geothermal reservoir stimulation. *Geothermics*, 76:93–105, 2018.
- [21] Jack H Norbeck, Mark W McClure, and Roland N Horne. Field observations at the fenton hill enhanced geothermal system test site support mixed-mechanism stimulation. *Geothermics*, 74:135–149, 2018.
- [22] Jack H Norbeck and David R Shelly. Exploring the role of mixed-mechanism fracturing and fluid-faulting interactions during the 2014 long valley caldera, california, earthquake swarm. *PROCEEDINGS Geothermal Reservoir Engineering Stanford University*, 2018.
- [23] Ayaka Abe, Roland N Horne, et al. Investigating the effect of wing cracks on the eggs reservoir permeability enhancement by hydraulic stimulation. In *ARMA-CUPB Geothermal International Conference*. American Rock Mechanics Association, 2019.
- [24] Ryan Schultz, Robert J Skoumal, Michael R Brudzinski, Dave Eaton, Brian Baptie, and William Ellsworth. Hydraulic fracturing-induced seismicity. *Reviews of Geophysics*, 58(3), 2020.
- [25] Serge Shapiro, R. Patzig, Elmar Rothert, and Jan Rindschwentner. Triggering of seismicity by pore-pressure perturbations: Permeability-related signatures of the phenomenon. *Pure and Applied Geophysics*, 160:1051–1066, 01 2003.
- [26] Pathikrit Bhattacharya and Robert Viesca. Fluid-induced aseismic fault slip outpaces pore-fluid migration. *Science*, 364:464–468, 05 2019.
- [27] Gillian R Foulger, Miles P Wilson, Jon G Gluyas, Bruce R Julian, and Richard J Davies. Global review of human-induced earthquakes. *Earth-Science Reviews*, 178:438–514, 2018.
- [28] Gail M Atkinson, David W Eaton, and Nadine Igonin. Developments in understanding seismicity triggered by hydraulic fracturing. *Nature Reviews Earth & Environment*, pages 1–14, 2020.
- [29] Richard Davies, Gillian Foulger, Annette Bindley, and Peter Styles. Induced seismicity and hydraulic fracturing for the recovery of hydrocarbons. *Marine and petroleum geology*, 45:171–185, 2013.
- [30] Shawn Maxwell. Unintentional seismicity induced by hydraulic fracturing. *CSEG Rec*, 38(8):40–49, 2013.
- [31] Corrie Clark, Andrew Burnham, Christopher Harto, and Robert Horner. Hydraulic fracturing and shale gas production: technology, impacts, and policy. *Argonne National Laboratory*, pages 1–16, 2012.
- [32] Rachel F Westwood, Samuel M Toon, Peter Styles, and Nigel J Cassidy. Horizontal respect distance for hydraulic fracturing in the vicinity of existing faults in deep geological reservoirs: a review and modelling study. *Geomechanics and geophysics for geo-energy and geo-resources*, 3(4):379–391, 2017.
- [33] Katie M Keranen and Matthew Weingarten. Induced seismicity. *Annual Review of Earth and Planetary Sciences*, 46:149–174, 2018.
- [34] Alan J Krupnick and Isabel Echarte. Induced seismicity impacts of unconventional oil and gas development. *Resources for the Future*, 2017.

- [35] P. A. Reasenberg and R. W. Simpson. Response of regional seismicity to the static stress change produced by the Loma Prieta earthquake. *Science*, 255:1687–1690, 1992.
- [36] Birendra Jha and Ruben Juanes. Coupled multiphase flow and poromechanics: A computational model of pore pressure effects on fault slip and earthquake triggering. *Water Resources Research*, 50(5):3776–3808, 2014.
- [37] X. Zhao and B. Jha. Role of well operations and multiphase geomechanics in controlling fault stability during CO₂ storage and enhanced oil recovery. *J. Geophys. Res.*, 1(21), 2019.
- [38] J. H. Dieterich. Modeling of rock friction, 1. Experimental results and constitutive equations. *J. Geophys. Res.*, 84:2161–2168, 1979.
- [39] J. H. Dieterich. Constitutive properties of faults with simulated gouge. *Mechanical Behaviour of Crustal Rocks: The Handin Volume, Geophys. Monogr. Ser.*, 24:108–120, 1981.
- [40] J. R. Rice, N. Lapusta, and K. Ranjith. Rate and state dependent friction and the stability of sliding between elastically deformable solids. *J. Mech. Phys. Solids*, 49:1865–1898, 2001.
- [41] Marion Y. Thomas, Nadia Lapusta, Hiroyuki Noda, and Jean-Philippe Avouac. Quasi-dynamic versus fully dynamic simulations of earthquakes and aseismic slip with and without enhanced coseismic weakening. *Journal of Geophysical Research: Solid Earth*, 119:1986–2004, 2014.
- [42] Lei Jin and Mark D. Zoback. Fully dynamic spontaneous rupture due to quasi-static pore pressure and poroelastic effects: An implicit nonlinear computational model of fluid-induced seismic events. *J. Geophys. Res.*, 123:9430–9468, 2018.
- [43] Mark W. McClure and Roland N. Horne. Investigation of injection-induced seismicity using a coupled fluid flow and rate/state friction model. *Geophysics*, 76:WC181–WC198, 2012.
- [44] Pedro Pampillon, David Santillan, Juan Carlos Mosquera, and Luis Cueto-Felgueroso. Dynamic and quasi-dynamic modeling of injection-induced earthquakes in poroelastic media. *J. Geophys. Res.*, 123:5730–5759, 2018.
- [45] Sara Aniko Wirp, Alice-Agnes Gabriel, Maximilian Schmeller, Elizabeth H Madden, Iris van Zelst, Lukas Krenz, Ylona van Dinther, and Leonhard Rannabauer. 3d linked subduction, dynamic rupture, tsunami, and inundation modeling: Dynamic effects of supershear and tsunami earthquakes, hypocenter location, and shallow fault slip. *Frontiers in Earth Science*, 9:177, 2021.
- [46] Eric O Lindsey, Rishav Mallick, Judith A Hubbard, Kyle E Bradley, Rafael V Almeida, James DP Moore, Roland Bürgmann, and Emma M Hill. Slip rate deficit and earthquake potential on shallow megathrusts. *Nature Geoscience*, 14(5):321–326, 2021.
- [47] Théa Ragon and Mark Simons. Accounting for uncertain 3-d elastic structure in fault slip estimates. *Geophysical Journal International*, 224(2):1404–1421, 2021.
- [48] Kali Allison, Laurent Montesi, and Eric Dunham. Earthquake cycles and shear zones: interplay between earthquakes, aseismic fault slip, and bulk viscous deformation. In *EGU General Assembly Conference Abstracts*, pages EGU21–13925, 2021.
- [49] SKY Lui, Y Huang, and RP Young. The role of fluid pressure-induced aseismic slip in earthquake cycle modulation. *Journal of Geophysical Research: Solid Earth*, 126(4):e2020JB021196, 2021.
- [50] Qingsheng Bai, Heinz Konietzky, Ziwei Ding, Wu Cai, and Cun Zhang. A displacement-dependent moment tensor method for simulating fault-slip induced seismicity. *Geomechanics and Geophysics for Geo-Energy and Geo-Resources*, 7(3):1–25, 2021.
- [51] J. R. Rice. Spatio-temporal complexity of slip on a fault. *J. Geophys. Res.*, 98:9885–9907, 1993.
- [52] Brad T Aagaard, Matthew G Knepley, and Charles A Williams. A domain decomposition approach to implementing fault slip in finite-element models of quasi-static and dynamic crustal deformation. *Journal of Geophysical Research: Solid Earth*, 118(6):3059–3079, 2013.
- [53] J. C. Jaeger and N. G. W. Cook. *Fundamentals of Rock Mechanics*. Chapman and Hall, London, 1979.
- [54] A. L. Ruina. Slip instability and state variable friction laws. *Geophys. Res. Lett.*, 88:359–370, 1983.
- [55] C. H. Scholz. Mechanics of faulting. *Ann. Rev. Earth Planet. Sci.*, 17:309–334, 1989.
- [56] C. Marone. Laboratory-derived friction laws and their application to seismic faulting. *Ann. Rev. Earth Planet. Sci.*, 26:643–696, 1998.
- [57] H Sun, H Waisman, and R Betti. A sweeping window method for detection of flaws using an explicit dynamic xfm and absorbing boundary layers. *International Journal for Numerical Methods in Engineering*, 105(13):1014–1040, 2016.

- [58] Jean-Pierre Berenger. A perfectly matched layer for the absorption of electromagnetic waves. *Journal of Computational Physics*, 114(2):185–200, 1994.
- [59] Ushnish Basu and Anil K. Chopra. Perfectly matched layers for time-harmonic elastodynamics of unbounded domains: theory and finite-element implementation. *Computer Methods in Applied Mechanics and Engineering*, 192(11-12):1337–1375, 2003.
- [60] T. C. Hanks and H. Kanamori. A moment magnitude scale. *J. Geophys. Res.*, 84:2348–2350, 1979.
- [61] Saumik Dana, Benjamin Ganis, and Mary F. Wheeler. A multiscale fixed stress split iterative scheme for coupled flow and poromechanics in deep subsurface reservoirs. *Journal of Computational Physics*, 352:1–22, 2018.
- [62] Saumik Dana and Mary F Wheeler. Design of convergence criterion for fixed stress split iterative scheme for small strain anisotropic poroelastoplasticity coupled with single phase flow. *arXiv preprint arXiv:1912.06476*, 2019.
- [63] Saumik Dana. System of equations and staggered solution algorithm for immiscible two-phase flow coupled with linear poromechanics. *arXiv preprint arXiv:1912.04703*, 2019.
- [64] Saumik Dana, Joel Ita, and Mary F Wheeler. The correspondence between voigt and reuss bounds and the decoupling constraint in a two-grid staggered algorithm for consolidation in heterogeneous porous media. *Multiscale Modeling & Simulation*, 18(1):221–239, 2020.
- [65] Saumik Dana, Xiaoxi Zhao, and Birendra Jha. Two-grid method on unstructured tetrahedra: Applying computational geometry to staggered solution of coupled flow and mechanics problems. *arXiv preprint arXiv:2102.04455*, 2021.
- [66] S. Dana and M. F. Wheeler. Convergence analysis of fixed stress split iterative scheme for anisotropic poroelasticity with tensor biot parameter. *Computational Geosciences*, 22(5):1219–1230, 2018.
- [67] S. Dana and M. F. Wheeler. Convergence analysis of two-grid fixed stress split iterative scheme for coupled flow and deformation in heterogeneous poroelastic media. *Computer Methods in Applied Mechanics and Engineering*, 341:788–806, 2018.
- [68] S. Dana. *Addressing challenges in modeling of coupled flow and poromechanics in deep subsurface reservoirs*. PhD thesis, The University of Texas at Austin, 2018.
- [69] Mohamad Jammoul, Mary F. Wheeler, and Thomas Wick. A phase-field multirate scheme with stabilized iterative coupling for pressure driven fracture propagation in porous media. *Computers & Mathematics with Applications*, 2021.
- [70] Mohamad Jammoul, Benjamin Ganis, and Mary F. Wheeler. General semi-structured discretization for flow and geomechanics on diffusive fracture networks. In *SPE Reservoir Simulation Conference*. Society of Petroleum Engineers, 2019.
- [71] B Aagaard, S Kientz, M Knepley, L Strand, and C Williams. Pylith user manual: version 2.1. 0. Davis, CA: *Computational Infrastructure of Geodynamics*, 2013.
- [72] Atgeirr Flø Rasmussen, Tor Harald Sandve, Kai Bao, Andreas Lauser, Joakim Hove, Bård Skaflestad, Robert Klöfkorn, Markus Blatt, Alf Birger Rustad, Ove Sævareid, et al. The open porous media flow reservoir simulator. *Computers & Mathematics with Applications*, 81:159–185, 2021.
- [73] Jiamin Jiang and Xian-Huan Wen. Smooth formulation for isothermal compositional simulation with improved nonlinear convergence. *Journal of Computational Physics*, 425:109897, 2021.
- [74] Yusuf Nasir, Oleg Volkov, and Louis J Durlofsky. A two-stage optimization strategy for large-scale oil field development. *Optimization and Engineering*, pages 1–35, 2021.
- [75] Jiawei Li, Pavel Tomin, and Hamdi Tchelepi. Sequential fully implicit newton method for compositional flow and transport. *Journal of Computational Physics*, page 110541, 2021.